
Article:
Hu, R., Wang, J.B. orcid.org/0000-0003-4870-3744, Mills, A. et al. (2 more authors) (2020) Current residual based stator inter-turn fault detection in permanent magnet machines. IEEE Transactions on Industrial Electronics. ISSN 0278-0046

https://doi.org/10.1109/tie.2020.2965500

Current Residual Based Stator Inter-Turn Fault Detection in Permanent Magnet Machines

Abstract— Inter-turn short circuit fault, also known as turn fault is a common fault in electric machines which can cause severe damages if no prompt detection and mitigation are conducted. This paper proposes a turn fault detection method for permanent magnet machines based on current residual. After the impact of the turn fault is firstly analyzed on a simplified mathematical machine model to assess the fault signature, a finite element (FE) model is developed to obtain healthy machine behavior. The residual between the measured and estimated currents by the model with the same applied voltages contains mainly the fault features. The quality of the fault detection can be improved because the fault signatures are enhanced, and the impact of the current controller bandwidth on fault signature is minimized. The dc components in the negative sequence current residuals are extracted through angular integration and their magnitude is defined as the fault indicator. The robustness of the fault detection against transient states is achieved. The effectiveness of the proposed method is validated on a triple redundant fault tolerant permanent magnet assisted synchronous reluctance machine (PMA SynRM).

***Index Terms*—Permanent magnet machine, turn fault detection, current residual, negative sequence, dc component extraction.**

I. INTRODUCTION

WITH the increasing application of electrical machines in safety-critical areas such as more electric aircrafts [1] and electric vehicles [2] , the reliability of the machine drive system is becoming more and more important. An unexpected fault or failure in the machine drives may lead to very high repair or replacement cost, or even catastrophic failure. Among all the possible failures that may occur in electrical machines, the stator winding faults can account for almost 25%, according to the industry survey described in [3]. It has been reported that most stator winding faults start from incipient inter-turn faults (or turn faults) [4] which occur due to insulation failures but develop into more serious inter-phase or phase-to-ground faults very quickly if no preventive measures or maintenance is taken. Insulation failures are attributed to excessive temperature, voltage stresses, vibration, environmental contamination, and aging. The large circulation current generated in the short-circuited paths may demagnetize the magnet irreversibly [5], and degrade the operating performance. More seriously, it also gives rise to a rapid increase in the temperature which accelerates the insulation deterioration process. The damage to the machine can be very quick and catastrophic. Thus, prompt and reliable diagnostic algorithms are essential, and have been extensively studied.

Various turn fault detection techniques have been proposed, and their merits and drawbacks, limitations and ambiguous points are extracted and compared in [6]. Among them, one of the most common techniques is based on the machine current signal analysis (MCSA) [7][8]. Since the symmetrical distribution of magnetic flux in a multi-phase machine in healthy operating condition is impaired by a turn fault, several unique harmonics emerge in the phase currents. It usually relies on the spectrum analysis tools such as fast Fourier transform (FFT) [9], which are limited to steady states. Short time Fourier transform (STFT) and wavelet transform (WT) [10] can be applied for the transient states, but the determination of the window length or the basic wavelet function, and the adaptability to different operating conditions are also of concern [11]. More advanced techniques Wigner-Ville distribution (WVD) [11], Hilbert-Huang transform (HHT) [12] can be used, but the computation complexity and time consumption are increased.

Apart from the featured frequency components in measured phase currents, the 2^{nd} harmonics in dq currents [13] and voltages are also favoured by many researchers [14]. They emerge in turn fault conditions because the symmetry in the three phase balanced systems is broken. Other methods based on the 2^{nd} harmonic of power [15], and Park's vector [16] can be seen as the extensions but with the same principle. Similarly, the negative sequence currents and voltages [17], which have been pointed out in [4] that they are equivalent to the 2^{nd} harmonic, are also widely researched for the turn fault detection. The largest faulted current can be generated with only one single turn fault which is usually seen as the most severe fault condition, however, the impact on the featured harmonics is the smallest, as has been stated in [18] . Under high driving currents or voltages, the accurate extraction of the fault signature can be more challenging, and the sensitivity of this method is reduced. Also, due to the closed-loop current control scheme that is usually applied to permanent magnet machines, these fault signatures might be impacted by the control bandwidth, but the issue is seldom addressed.

In [19], search coils are installed in the stator teeth, and the induced voltage is used to detect turn fault. However, they are invasive. Diagnostic methods based on high frequency (HF) signal injection techniques are proposed in [20] where, the featured HF components are transformed to a low frequency range, and their negative-sequence components are used as the fault indicators. In [21], zero sequence voltage and current are also employed for the detection of turn fault, where their fundamental components are utilized albeit the access to the winding neutral point is required.

Residual current, voltage, or back electromotive force(EMF)

[22][23] are also exploited for the detection of turn fault if an accurate model depicting normal machine behaviour is available. The model can be established from lumped parameters, finite element analysis, or even trained neutral network [24]. Residual current vector (RCV) based turn fault detection methods are proposed in [25][26], where the stator currents are estimated by using a state observer. However, the effects of transient speed and load conditions on the detection performance has not been addressed.

In this paper, a new turn fault detection method is proposed by detecting the negative sequence components in the current residuals. It combines the two types of methods that are based on the negative sequence components and the current residual respectively, so as to benefit simultaneously of the advantages of both approaches. Since the accurate machine model is always difficult to obtain, errors are inevitable. As the consequence, the residual current is not equal to zero in healthy states but may vary with operating conditions. For a given robustness, the sensitivity is highly dependent on the modelling. However, the benefit of using current residual is that the fault signature of the negative sequence component is preserved, while the main components are eliminated in the current residual. Thus, the fault signature is relatively enhanced, which makes it more sensitive to turn fault and more convenient to be detected.

A finite element model of the machine in healthy conditions is firstly established to generate the current estimations with given dq voltage references. Through the comparison with the current measurements, the current residuals are then produced, where the fault signatures are enhanced, since other unwanted components are eliminated. After transforming into the backward rotating frame, angular integration is applied to extract the dc values of the negative sequence components. The magnitude of the dc components of the current residual vector is then defined as the fault indicator. The impact of the transient states can be, therefore, minimized. As a result, a single turn fault with a benign fault signature can be detected more reliably in both steady and transient state operations.

The rest of this paper is organized as follows. In section II, a simplified machine model in turn fault conditions is analyzed mathematically to assess the fault signature. In section III, an FE model of the machine in healthy conditions is utilized to generate the current residuals in actual implementation. Section IV proposes the turn fault detection procedure. Experimental results and conclusions are given in section V and section VI, respectively.

II. MACHINE BEHAVIOR UNDER INTER TURN FAULT CONDITION

A. Fault current

The turn fault occurs when different turns in a coil begin to contact each other due to insulation breakdown. If the insulation degradation is severe, the contact resistance can be very low, which forms a short-circuit path. When the contact resistance reaches zero in the extreme case, that part of the coil conductors is fully short circuited.

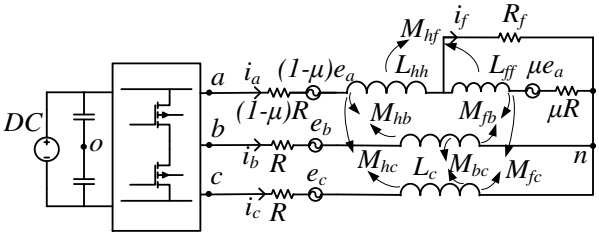

Fig. 1. Equivalent circuit and parameters in turn fault condition

Without loss of generality, the turn fault is assumed to be in phase A, whose winding is divided into healthy and faulted parts, as shown in Fig. 1. The contact resistance is denoted as R_f. The ratio of the number of the short-circuited turns over the total number of the series turns in one phase is defined as μ, which represents the fault range between 0 and 1. The self-inductances in the healthy and faulted parts, and the mutual inductance between them are also defined. Since the back EMF can be considered proportional to the number of turns, the EMFs in healthy and faulted parts can be calculated accordingly.

Based on the equivalent circuit, the model under fault conditions can be expressed in (1), where u_{ah} and u_{af} denote the voltages in the healthy and faulted parts of phase A winding, respectively, i_f denotes the fault current caused by the short circuit, and λ_a , λ_b , and λ_c are the permanent magnet (PM) flux linkage in phases A, B, and C, respectively.

$$\mathbf{U}_s^{tf} = \mathbf{R}_s^{tf}\mathbf{i}_s^{tf} + \frac{d(\mathbf{L}_s^{tf}\mathbf{i}_s^{tf} + \boldsymbol{\lambda}_{PM}^{tf})}{dt} \tag{1}$$

where $\mathbf{U}_s^{tf} = \begin{bmatrix} u_{ah} & u_{af} & u_{bn} & u_{cn} \end{bmatrix}^T$, $\mathbf{i}_s^{tf} = \begin{bmatrix} i_a & i_a - i_f & i_b & i_c \end{bmatrix}^T$

$$\mathbf{L}_s^{tf} = \begin{bmatrix} L_{hh} & M_{hf} & M_{hb} & M_{hc} \\ M_{hf} & L_{ff} & M_{fb} & M_{fc} \\ M_{hb} & M_{fb} & L_b & M_{bc} \\ M_{hc} & M_{fc} & M_{cb} & L_c \end{bmatrix}, \boldsymbol{\lambda}_{PM}^{tf} = \begin{bmatrix} 1-\mu & & & \\ & \mu & & \\ & & 1 & \\ & & & 1 \end{bmatrix} \begin{bmatrix} \lambda_a \\ \lambda_a \\ \lambda_b \\ \lambda_c \end{bmatrix}$$

$$\mathbf{R}_s^{tf} = R\begin{bmatrix} 1-\mu & \mu & 1 & 1 \end{bmatrix},$$

where, R, L and M are the phase resistance, self- and mutual inductances as defined in Fig 1.

According to [27] and [28], the following relationship between the self and mutual inductances related with the faulted turns can be obtained, shown in (2).

$$\begin{aligned} L_{hh} + 2M_{hf} + L_{ff} &= L_a \\ M_{hb} + M_{fb} &= M_{ab} \\ M_{hc} + M_{fc} &= M_{ac} \\ M_{hf} + L_{ff} &= \mu L_a \\ M_{fb} &= \mu M_{ab} \\ M_{fc} &= \mu M_{ac} \end{aligned} \tag{2}$$

Rearrange the phase voltage equations by applying $u_{an}=u_{ah}+u_{af}$ the three phase voltage equations in turn fault conditions can be derived and is given in (3).

$$\begin{aligned} \mathbf{U}_s = R\mathbf{i}_s + \frac{d(\mathbf{L}_s\mathbf{i}_s + \boldsymbol{\lambda}_{PM})}{dt} \\ - \mu R\begin{bmatrix} i_f & 0 & 0 \end{bmatrix} - \mu\frac{d\left(\begin{bmatrix} L_a & M_{ab} & M_{ac} \end{bmatrix}^T i_f\right)}{dt} \end{aligned} \tag{3}$$

where $\mathbf{U}_s = \begin{bmatrix} u_{an} & u_{bn} & u_{cn} \end{bmatrix}^T$, $\mathbf{i}_s = \begin{bmatrix} i_a & i_b & i_c \end{bmatrix}^T$

$$\mathbf{L}_s = \begin{bmatrix} L_a & M_{ab} & M_{ac} \\ M_{ba} & L_b & M_{bc} \\ M_{ca} & M_{cb} & L_c \end{bmatrix}, \boldsymbol{\lambda}_{PM} = \begin{bmatrix} \lambda_a \\ \lambda_b \\ \lambda_c \end{bmatrix}$$

In addition, the voltage and flux linkage of the faulted part can be expressed in (4) and (5). For a given number of short-circuited turns, the lower R_f is, the larger i_f can reach, leading to a worse scenario. Thus, to evaluate the most severe condition and for the sake of simplicity, R_f is assumed zero in the subsequent analysis.

$$u_f = R_f i_f = \mu R(i_a - i_f) + \frac{d\lambda_f}{dt} \tag{4}$$

$$\lambda_f = \mu \begin{bmatrix} L_a & M_{ab} & M_{ac} \end{bmatrix} \mathbf{i}_s - \mu^2 L_a i_f + \mu \lambda_a \tag{5}$$

It can be deduced from the expressions above that i_f is a function of i_a, i_b, i_c, and the time derivative of λ_a. With high-order harmonics neglected, the fault current i_f can be expressed in (6), where θ_e is the rotor electrical angle, I_{f1} denotes the amplitude, and is dependent on machine speed. θ_1 is the associated phase angle.

$$i_f \approx I_{f1} \sin(\theta_e + \theta_1) \tag{6}$$

B. Influence of turn fault on dq currents

When the three phase quantities are transformed into the rotating dq frame, the dq voltages can be expressed in (7). Compared with the healthy machine model under the same dq currents, the additional terms, Δu_{df} and Δu_{qf}, caused by the turn fault can be observed. They constitute the fault signatures in the dq voltages. The interactions of the fault current given in (6) with the $\sin\theta_e$ and $\cos\theta_e$ terms in Δu_{df} and Δu_{qf} produce a dc component, and 2nd harmonics in the dq voltages, as given in (8). The first term is associated with the change of the positive-sequence voltage, whereas the second term is associated with the change of negative-sequence voltage due to the fault. The subscript "dc" denotes dc component, and "2nd" denotes 2nd harmonic.

$$\begin{cases} u_d = R_s i_d + L_d \dfrac{di_d}{dt} - \omega_e L_q i_q + \Delta u_{df} \\ u_q = R_s i_q + L_q \dfrac{di_q}{dt} + \omega_e (L_d i_d + \lambda_{pm}) + \Delta u_{qf} \\ \Delta u_{df} = +\dfrac{2}{3}\mu\omega_e L_d i_f \sin\theta_e - \dfrac{2}{3}\mu L_d \cos\theta_e \dfrac{di_f}{dt} \\ \qquad -\dfrac{2}{3}\mu\omega_e L_q i_f \sin\theta_e - \dfrac{2}{3}\mu R i_f \cos\theta_e \\ \Delta u_{qf} = +\dfrac{2}{3}\mu\omega_e L_q i_f \cos\theta_e + \dfrac{2}{3}\mu L_q \sin\theta_e \dfrac{di_f}{dt} \\ \qquad -\dfrac{2}{3}\mu\omega_e L_d i_f \sin\theta_e + \dfrac{2}{3}\mu R i_f \cos\theta_e \end{cases} \tag{7}$$

$$\begin{cases} \Delta u_{df} \approx \Delta u_{df\_dc} + \Delta u_{df\_2nd} \\ \Delta u_{qf} \approx \Delta u_{qf\_dc} + \Delta u_{qf\_2nd} \end{cases} \tag{8}$$

$$\begin{aligned} u_d &= R_s i_d' + L_d \frac{di_d'}{dt} - \omega_e L_q i_q' \\ u_q &= R_s i_q' + L_q \frac{di_q'}{dt} + \omega_e (L_d i_d' + \lambda_{pm}) \end{aligned} \tag{9}$$

$$\begin{aligned} i_d' &= i_d - \frac{2}{3}\mu i_f \cos\theta_e \\ i_q' &= i_q + \frac{2}{3}\mu i_f \sin\theta_e \end{aligned} \tag{10}$$

If the same voltages given in (7) are applied to the machine model equations of (9) in healthy conditions, then the dq currents can be calculated and expressed in (10), where i_d' and i_q' denote the predicted dq currents with the machine model under healthy conditions. Thus, the change in the dq currents due to the fault under the same applied dq voltages can also be used as fault signatures.

It should be noted that the simplified mathematical models in the healthy and turn fault conditions in this section are utilized to assess the fault signatures qualitatively, i.e. the change in both the dc components and 2nd harmonics in the dq voltages and currents. For the actual implementation, only a high fidelity model based on finite element analysis in healthy conditions is required, as will be detailed in the following section.

III. DQ CURRENT RESIDUALS ACQUIRED FROM MACHINE MODEL

It can be concluded that the dq voltage equations of the machine under turn fault conditions are different from that in healthy conditions. Thus, if the machine model in healthy operations can be obtained in actual implementation, the voltages in healthy condition can be estimated with the measured currents. By comparing the actual voltages with the estimation, the voltage residual can indicate whether a turn fault has occurred. However, the voltage estimation requires computing the derivatives of the flux linkages, which can be prone to noise because of PWM operation of the inverter.

To avoid such problem, the dq currents are estimated, with the mathematical model in (11) employed. The dq flux linkages are first calculated by the integration of the net voltages shown in the first and second equations in (11). Then, the inverse flux linkage functions are used to obtain the dq currents with the estimated dq flux linkages and the measured rotor position [29]. The inverse is calculated by the flux linkages as functions of the dq currents and rotor position angle obtained from finite element analysis in advance. This is necessary because for an interior permanent magnet machine, the dq inductances and flux linkages are not only dependent on rotor position, but also affected by dq currents.

By way of example, Fig. 2 shows the inverse dq current maps versus the dq flux linkages at 0° rotor position. Together with the measured dq currents, the current residual can be obtained, which should be close to zero in healthy condition if the model is sufficiently accurate. From the analysis in (9) and (10), the current residual in the fault condition representing the difference between the healthy and faulted machine behaviours can be expressed in (12), where the original fault signatures in the currents are extracted. The superscript p denotes the positive sequence rotating dq frame. It can be deduced that the current residuals are only related to the fault current and the percentage of the short circuited turns, and is independent of the current controller bandwidth.

$$\begin{cases} \lambda_d = \int (u_d - R_s i_{d\_e} + \omega_e \lambda_q) dt \\ \lambda_q = \int (u_q - R_s i_{q\_e} - \omega_e \lambda_d) dt \\ i_{d\_e} = f^{-1}(\lambda_d, \lambda_q, \theta_m) \\ i_{q\_e} = g^{-1}(\lambda_d, \lambda_q, \theta_m) \end{cases} \tag{11}$$

$$\begin{aligned} i^p_{d\_re} &= i_d - i_{d\_e} = +\frac{2}{3}\mu i_f \cos\theta_e \approx i^p_{d\_re\_dc} + i^p_{d\_re\_2nd} \\ i^p_{q\_re} &= i_q - i_{q\_e} = -\frac{2}{3}\mu i_f \sin\theta_e \approx i^p_{q\_re\_dc} + i^p_{q\_re\_2nd} \end{aligned} \tag{12}$$

Whereas phase currents are usually measured in a drive system, voltage transducers are not necessary for drive control. In order to avoid the use of extra voltage transducers, the voltages for the input to the model are estimated by the dq voltage commands from the output of the current controller. The desired voltages should be equal to the voltage demands in the linear mode of SVPWM. However, in the nonlinear mode, when the modulation index is high, their relationship depends on the overmodulation strategy, and the actual voltages can still be estimated by the voltage commands accordingly. The non-linear characteristics of the inverter including the voltage drop of the devices and the dead time effects result in the voltages applied to the machine and to the model being different. Also, with the consideration that small errors might also exist in the mathematical model, the current residual may deviate from zero even in healthy conditions. Therefore, by simply comparing the dq current residual to zero is not a good solution for fault detection.

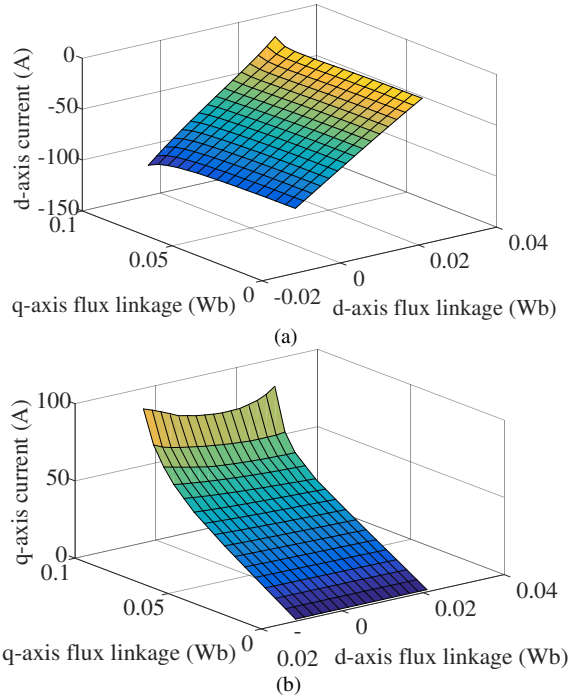

Fig. 2 Current maps versus d- and q-axis flux linkages at rotor position =0°. (a) d-axis current. (b) q-axis current.

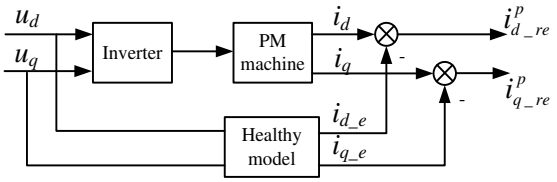

Fig. 3 Current residual generation scheme

If the machine is balanced in three phases in healthy conditions, those errors in the voltages and machine models only add to the dc components and higher order harmonics in the dq current residuals while no 2nd harmonics will be introduced. Therefore, the 2nd harmonic in the current residual can be used as a good fault indicator according to (12). Since the dc components in the dq current residuals are greatly eliminated by the estimation, the 2nd harmonic is more pronounced in the current residuals under the fault condition, thereby improving signal-to-noise ratio of the fault detection process. Thus, the turn fault detection should be based on the 2nd harmonic of the positive sequence dq current residual, as expressed in (13).

$$FI^p = \begin{bmatrix} i^p_{d\_re\_2nd} \\ i^p_{q\_re\_2nd} \end{bmatrix} \tag{13}$$

IV. FAULT DETECTION

Various frequency components extraction techniques can be applied for the detection of the 2nd harmonic in the positive sequence dq current residual. Alternatively, the current residuals in the positive rotating dq frame can be transformed into the backward (negative) rotating dq frame, then the fault indicator of the 2nd harmonic is converted into the dc value of the negative sequence components, as shown in (14). To maximize detection sensitivity, the magnitude of the dc values of the negative sequence dq current residuals, given in (15), is defined as the fault indicator. Thus, the turn fault detection is mainly based on the extraction of the dc components, where the superscript *n* denotes negative sequence components.

$$\begin{aligned} \begin{bmatrix} i^n_{d\_re} \\ i^n_{q\_re} \end{bmatrix} &= \begin{bmatrix} \cos 2\theta_e & -\sin 2\theta_e \\ \sin 2\theta_e & \cos 2\theta_e \end{bmatrix} \begin{bmatrix} i^p_{d\_re} \\ i^p_{q\_re} \end{bmatrix} \\ &= \begin{bmatrix} i^n_{d\_re\_dc} + i^n_{d\_re\_2nd} \\ i^n_{q\_re\_dc} + i^n_{q\_re\_2nd} \end{bmatrix} \end{aligned} \tag{14}$$

$$FI^n = \sqrt{{i^n_{d\_re\_dc}}^2 + {i^n_{q\_re\_dc}}^2} \tag{15}$$

In a real machine drive system, the back EMF and non-ideal inverter as well as magnetic saturation and rotor saliency will introduce higher order harmonics even in healthy conditions. In the negative rotating dq frame, these harmonics can coexist with the 2nd harmonic due to the model inaccuracy. Only the dc component of the residual current in the negative rotating frame is the indicator of a turn fault, thus all other harmonics need to be eliminated. Low pass filters or notch filters can be used to filter out the harmonics, but the filter parameters need to vary with operating frequency. When the speed or frequency is varying, the filter response and, hence the quality of detection deteriorates.

Since the rotor position angle is always available for the PM machine drive systems, the dc component can be estimated

more accurately within one electrical cycle, regardless of speed or frequency change. Through the integration of the negative sequence current residual within 2π electric radians shown in (16), all the harmonics can be eliminated, and the dc component can be obtained exclusively. Thus, the integration results and then the fault indicator in (15) should be zero in healthy conditions, but nonzero in turn fault conditions. A threshold can be determined empirically based on the experimental observations in healthy conditions. And if the fault indicator is higher than the threshold, a turn fault is detected.

$$\begin{bmatrix} i_{d\_re\_dc}^{n} \\ i_{q\_re\_dc}^{n} \end{bmatrix} = \frac{1}{2\pi}\int_{\theta_e-2\pi}^{\theta_e} \begin{bmatrix} i_{d\_re}^{n}(\theta_e) \\ i_{q\_re}^{n}(\theta_e) \end{bmatrix} d(\theta_e) \qquad (16)$$

It should be noted that the angular integration based dc component extraction and the fault detection based on the comparison with the threshold work well in both steady and speed transient states. However, if there is a current (or load torque) transient, causing the varying magnitude of the negative sequence current residual, then the integration results may fluctuate. Thus their magnitude might also be higher than the predefined threshold for a period even in healthy condition, and a false alarm might be triggered. However, the magnitude can quickly decrease to below the threshold in healthy conditions due to the fluctuation. In order to avoid false alarms, a load transient evaluation process is included in the fault detection process.

Once the fault indicator exceeds the threshold, then an angle counter is activated and records the angle increment. Otherwise, the counter is reset to zero. If the angle recorded in the counter is always small than the predefined transient evaluation period, then it should due to the fluctuation caused by a load transient. Conversely, if the counter is greater than such period, then it should be caused by the turn fault. The determination of this evaluation period is a tradeoff between the risk of false alarm and the detection response time, and can be determined as 2π according to the test results. Based on the above description of the fault signature extraction with the consideration of load transients, the whole signal processing and turn fault detection flow chart is shown in the upper and lower parts of Fig. 4, respectively.

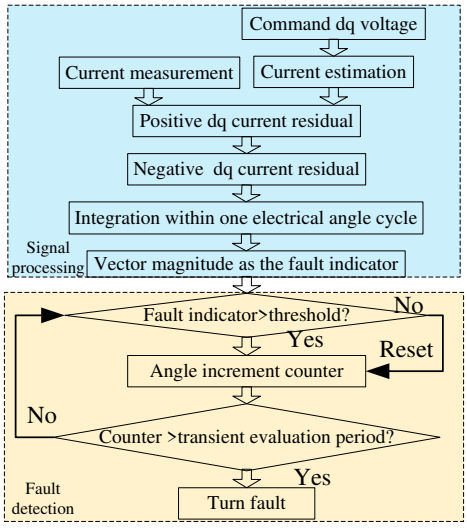

Fig. 4 Fault detection flow chart

V. EXPERIMENTAL TESTS

A fault tolerant machine drive based on permanent magnet assisted synchronous reluctance machine (PMA SynRM) is used for the validation of the proposed fault detection method. The machine has 36 slots and 3 pole pairs, with three independent 3-phase windings, which are segregated into triple redundant 3-phase winding configuration, as shown in Fig. 5. Since there is no overlap between two different 3-phase winding sets, the risk of short circuit fault in two 3-phase sets is largely reduced. Also, the degradation or failure on one 3-phase winding is not likely to transmit to other 3-phase windings, because the heat generated is more likely to be spread around radially due to the higher thermal conductivity of the stator iron. Each 3-phase winding set, ABC, DEF, and GHI forms a balanced 3-phase system in space and time, and is controlled independently by three separate inverters in the same way as a 3-phase IPM machine. Such physical, thermal and electrical isolation guarantees the fault tolerant capability when a fault occurs in one 3-phase winding set and a mitigation action is taken, while the other two 3-phase winding sets are still operational to provide the torque. The machine specification is shown in Table I. The test rig set up is shown in Fig. 6. According to [18], in the turn fault case with lower ratio of the number of short circuited turns to the total number of the series connected turns in a phase, the short circuit current is larger and hence the severity is higher. However, the 3-phase system is less unbalanced, and the conventional fault signatures can be lower. Therefore, the detection of one single turn short-circuit fault is essential but most challenging, and is tested in the experiments. A single turn short-circuit fault in coil B2 of the 3-phase winding set ABC is emulated by controlling a relay, which has introduced 1.4 mΩ resistance in the short circuit path. Due to the current limit of the relay, all the fault detection tests are conducted below 1000 rpm for the sake of safety.

TABLE I MACHINE SPECIFICATIONS

Specification	Symbol	Value
Base speed	n_b	4000 rpm
Maximum speed	n_m	19200 rpm
Rated power	P_r	35 kW
Rated current	I_{rated}	120 A peak
Nominal DC link voltage	V_{dc}	270 V
Turn number of each coil	N	8
Number of faulted turns	N_f	1
PM flux linkage	λ_{pm}	0.025 Wb
Phase resistance	R_s	0.025 Ω
d-axis inductance (nominal)	L_d	0.38 mH
q-axis inductance (nominal)	L_q	1.02 mH

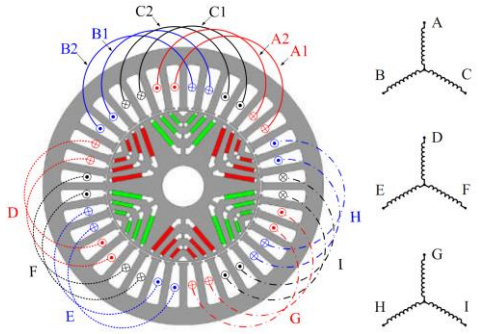

Fig. 5 Triple redundant PMA SynRM with segregated windings

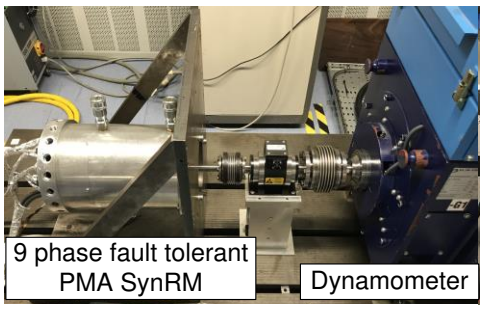

(a)

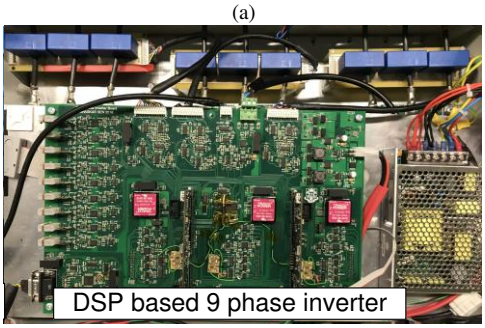

(b)

Fig. 6 (a)The nine phase PMA SynRM test rig. (b)DSP controlled nine phase inverter.

A. Validation of the machine mathematical model

In order to improve sensitivity and robustness of the fault detection, the signatures in the current residual which are not caused by the fault should be eliminated. Hence, the error of the mathematical model which is not related to the fault needs to be small. Thus, the accuracy of the machine model is examined first.

Fig. 7 shows the estimated and measured dq currents denoted as 'est' and 'mea', respectively, and the negative sequence dq current residuals at different speeds in healthy condition when the phase current amplitude is 80 A. According to the maximum torque per ampere (MTPA) control scheme, the given i_d reference is -53.5 A and the i_q reference is 59.5 A. As can be seen, the measured dq currents do not contain any significant harmonics under current feedback control. The harmonics shown in the estimated currents result from distortions in the command dq voltages, which are caused by high order harmonics in the back EMF and slotting effect as well as non-linear machine behaviour. The errors in the current estimation can be seen more significant at lower speed but are much reduced at the higher speed of 1000 rpm. Therefore, the accuracy of the current estimation improves at high speed. This error is mainly caused by the difference between the command voltages and the actual voltages due to the inverter voltage nonlinearity effect. According to [30], such nonlinearity effect on the machine performance at a low-speed region are especially more severe than those at a high-speed region. As a result, the current prediction can be more accurate at high speeds.

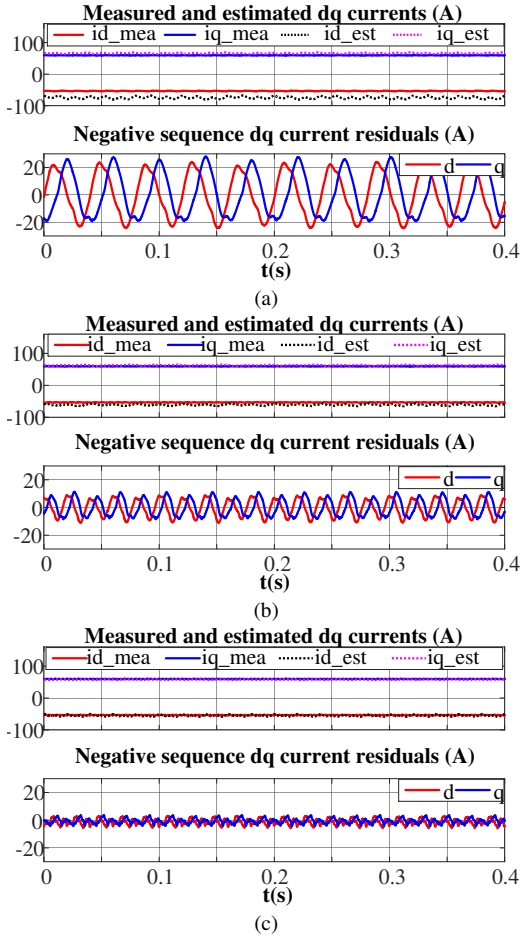

Fig. 7 The performance of current estimation by machine model at 80 A (i_d = -53.5 A, i_q = 59.5 A) at different speeds (a)250 rpm (b) 500 rpm (c)1000 rpm

B. Influence of controller bandwidth

Conventional signals such as the measured dq currents or the command dq voltages can also be used to extract the 2nd harmonic or the equivalent negative sequence components for the fault detection. However, the magnitude of the 2nd harmonic is affected by the current controller bandwidth. In contrast according to (12), the current residuals are only related to the fault current and the percentage of the shorted turns, and are independent of the controller bandwidth. In order to validate this point, experimental tests with different bandwidths are also conducted. The machine is operating at 1000 rpm with 50 A phase current (i_d=-28.7 A, i_q=41 A). The tested bandwidths are 400 Hz and 800 Hz. The positive sequence measured dq currents, command dq voltages, and dq current residuals are compared in Fig. 8(a), (b) and (c) respectively, when a single turn fault is injected at 0.11s. It can be observed that with the increase of the bandwidth, the 2nd harmonics in the measured dq currents decrease in the fault conditions whilst the 2nd harmonics in the command dq voltages increase, even though they are at different magnitudes. However, very little change is observed in the dq current residuals. These characteristics with the change of bandwidth can apply to other operating conditions. Therefore, the effect of the current controller bandwidth on the current residual based fault indicator is minimized, while the fault signatures are enhanced.

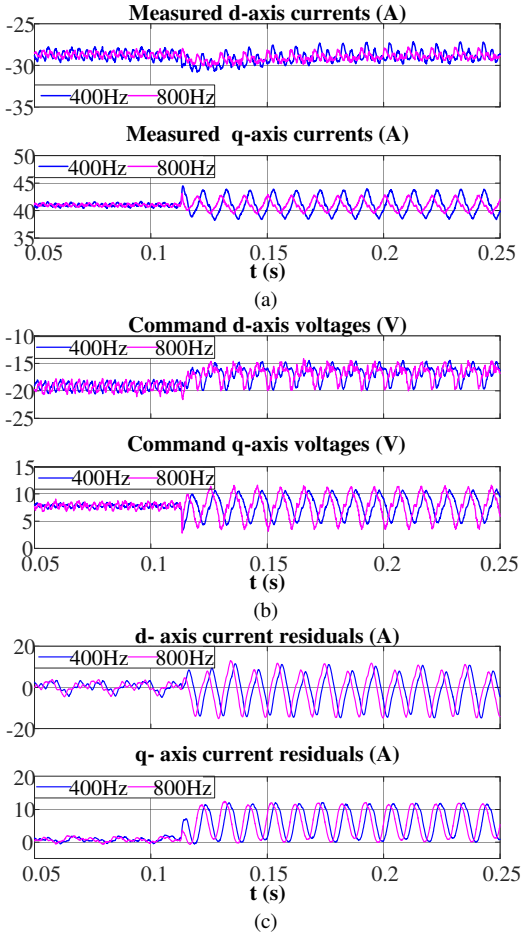

Fig. 8 Comparisons of the positive sequence (a) measured dq currents (b) command dq voltages (c) dq residual currents at 1000 rpm 50 A with different current controller bandwidths

C. Fault current

When the machine is operating at 1000 rpm with 70 A phase current under MTPA control, and a single turn fault, which has the most benign fault signature, is activated at 0.11 s, the fault current flowing through the short-circuited path is shown in Fig. 9. It can be observed that the fault current mainly contains the fundamental component and 3rd harmonic, and its peak value can reach more than 300 A or 2.5 p.u.. The RMS value of the rated current is about 85 A, and the RMS value of the fault current at different speeds and phase currents are recorded and given in Fig. 10. It is evident that the fault current increases with either the speeds or load currents. At low speed with low current, the fault current is also lower than the rated current.

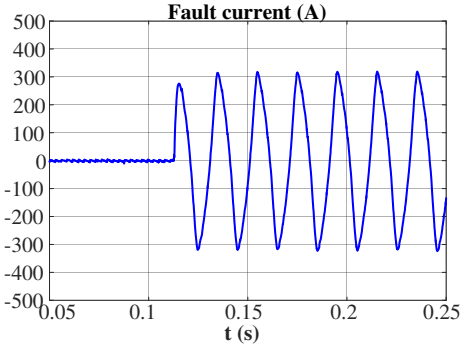

Fig. 9. Fault current waveform at 1000rpm with 70A phase current

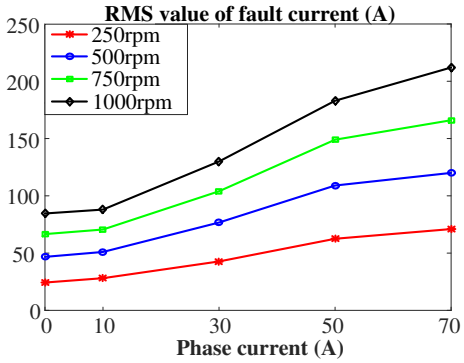

Fig. 10. Variations of the RMS fault current with speed and current

D. Fault detection in steady state

When the machine is operating at 500 rpm with 50 A phase current (i_d=-28.7 A, i_q=41 A), and a single turn fault occurs at 0.11 s, the detection results are shown in Fig. 11. The 2nd harmonics start to appear in the command dq voltages, measured and estimated dq currents. The 2nd harmonics as the fault signatures are preserved during the calculation of current residuals and are transformed into dc components in the negative rotating dq frame. The dc components of both negative sequence d and q current residuals are extracted by angular integration, and their vector magnitude is compared with the threshold. When it exceeds the threshold, the angle counter is activated. When the counter reaches 2π, which indicates that the vector magnitude of the dc components is persistently greater than the threshold, the fault is detected effectively. The time duration for this process is about 0.04 s for 500 rpm.

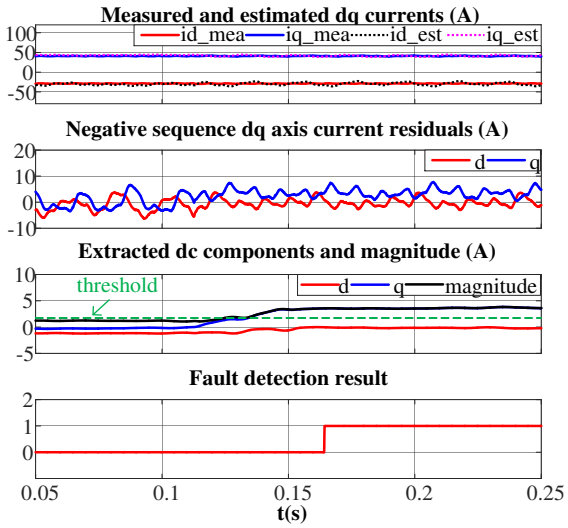

Fig. 11 Fault detection process and result

To demonstrate the benefit of implementing the machine model to obtain the current residual, the fault signatures extracted from the measured dq currents and command dq voltages without the use of the machine model, and the current residuals with the model are compared at 1000 rpm with 50 A. Although the fault indicators in [13] and [14] are normalized against the positive sequence components, it is still essential to obtain a favourable negative sequence components results in the first place with good stability and distinct change. The same fault as described previously is injected at 0.11s and the same angular integration technique is used for the extraction of the negative sequence components. It can be observed from Fig. 12

(a) that the magnitude of the dc component vector extracted from the negative sequence measured dq currents exhibit excessive fluctuation which would lead to incorrect detection response. Also, the deviation of the dc vector magnitude in the fault condition is small. It is, therefore, difficult to set an appropriate threshold to differentiate the healthy and faulted conditions. Although the fault signatures are increased slightly in the negative sequence command dq voltages shown in Fig. 12 (b), the fault detection sensitivity is still compromised due to the fluctuations and indistinctive change in the turn fault conditions. With the application of the machine model to generate the current residuals, the extracted negative sequence dc components and the vector magnitude shown in Fig. 12 (c) are much less volatile and more pronounced due to the suppression of the unwanted components, thus, the sensitivity and robustness of fault detection using the current residual can be largely enhanced.

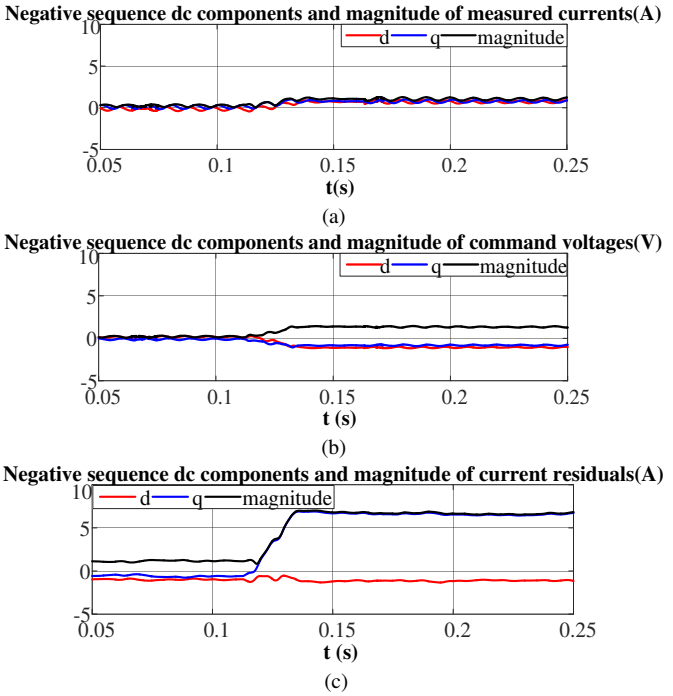

Fig. 12. Negative sequence dc components and magnitude of (a) measured dq currents, (b) command dq voltages, (c) dq current residuals at 1000 rpm, 50 A

For different operating conditions, the magnitudes of the negative sequence dq current residuals vector are shown in Fig. 13, where 'H' denotes healthy conditions and 'TF' denotes turn fault conditions. As can be seen, in healthy conditions, the fault indicator is not zero, but is slightly dependent on the load current. This is mainly caused by the inherent impedance unbalance among the three phases in the test machine. The small inherent unbalance can be accounted by setting up appropriate threshold in the detection logic. In turn fault conditions, deviations of the fault indicator from the healthy conditions are observed, and increase proportionally with the speed and current. Thus, the detection at very low speeds and currents are less sensitive. Based on the test results, a threshold as the function of current should be defined. With the consideration of measurement noise and error, a margin of 0.5 A is set for the determination of the threshold in this case. It can be deduced that the turn fault in any operating conditions with the speed no lower than 250 rpm and the current no lower than 10A can be detectable. When examining the no load (0 A) conditions, it is clear that the turn fault at 750 rpm and 1000 rpm speeds can still be detected. This is different from the MCSA based fault detection method, which is no longer applicable under no load conditions due to the loss of current signals. However, the fault signatures are still preserved in the command dq voltages, which are transferred to the current residuals, making the fault detection still effective, even if the phase currents are zero. When the speed is as low as 500 rpm and 250 rpm with 0 A current, the fault indicator is too small, and the fault cannot be detected. Nevertheless, the fault current is also relatively low (<50A) at such low speeds according to Fig. 10, and the risk of causing damage to the machine can be neglected. Thus, the overall detection zone can be obtained, as shown in (17), where I is the phase current magnitude, and ω_r is the rotating speed.

$$\{(\omega_r, I) | 250rpm \le \omega_r \le 750rpm, I \ge 10A\} \cup \{(\omega_r, I) | \omega_r \ge 750rpm, I \ge 0A\} \quad (17)$$

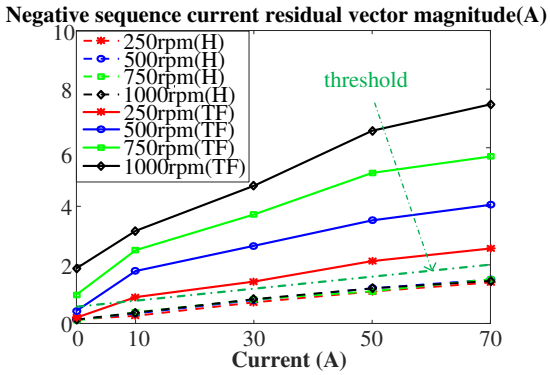

Fig. 13. Variations of negative sequence dq current residuals vector magnitude with speed and current in healthy and turn fault conditions

E. Fault detection during transients

The turn fault detection during transient states and the effectiveness of angular integration based dc component extraction are also tested.

Firstly, the test is performed with acceleration set to 1000 rpm/s via the dynamometer when the machine is initially operating at 700 rpm and 50 A load current, and the resultant speed and detection response in the healthy condition are shown in Fig. 14 (a). With the angular integration based order tracking, the processing interval is always kept to one electrical cycle regardless of the speed change. Thus, the extracted negative sequence dc components and their vector magnitude are not affected. In this way, false alarms can be avoided. When the fault occurs during the acceleration shown in Fig. 14 (b), it can be detected as swiftly as in steady state operations.

Secondly, the effect of the current step change in healthy condition on the proposed detection method is tested and illustrated in Fig. 15(a). The speed is controlled by the dynamometer at 250 rpm initially and a step change in load current from 20 A to 80 A is applied at 0.2 s. Due to the limited response time of the dynamometer, the sudden change in the torque cause small deviations and fluctuations of the speed. The current step change leads to the magnitude variation of the dq current residuals, and hence the magnitude variation of the 2nd harmonics in the negative sequence dq current residuals. As can

be seen, when the angular integration is performed, the extraction of dc component is affected by this variation, and the fluctuation in the calculated vector magnitude of the dc components is seen. Although, the magnitude of the dc component vector can cross the threshold for a while when the angle counter starts accumulating from zero, it will decrease to below the threshold due to fluctuation, causing the angle counter to reset. Eventually, the angle counter never exceeds the determined transient evaluation period of 2π. Thus, according to the fault detection steps in Fig. 4, this load transient condition will not cause a false alarm. When the fault occurs at 0.21 s during the load transient as shown in Fig. 15 (b), the fault detection is effective, since the magnitude of the dc component vector has been over the threshold for the evaluation period.

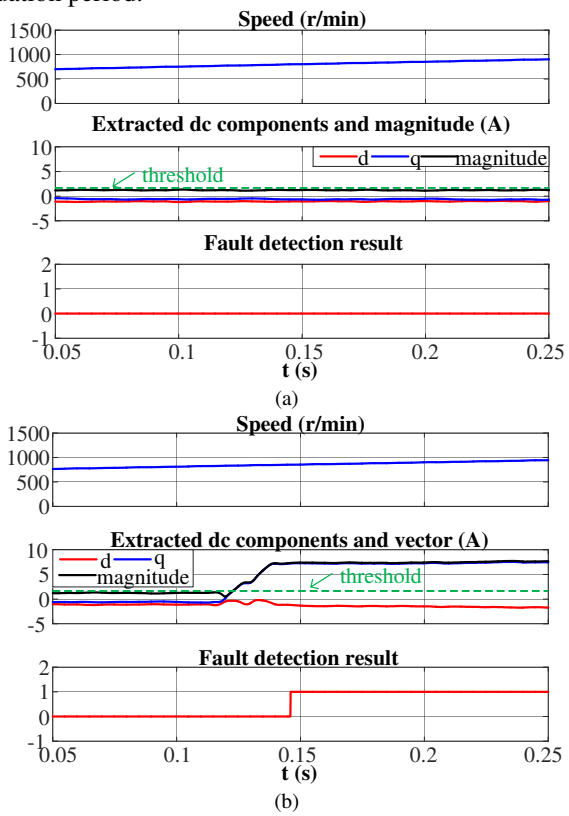

Fig. 14 The effect of varying speed on the fault detection result in (a) healthy and (b) fault condition

VI. Conclusions

A turn fault detection technique based on negative sequence dq current residuals by employing the machine model has been proposed. It has been demonstrated that the fault signatures can be enhanced and detection sensitivity improved when most of the unwanted components are eliminated in the current residuals. The influence of the control bandwidth on the fault signature has also been minimized. The fault indicator is defined as the magnitude of the negative sequence dc components of the dq current residuals, which are extracted by the angular integration. As the result, the influence of the model errors, other harmonics and the speed transients on turn fault detection are minimized. A complete turn fault detection procedure with the consideration of the discrimination of load transient states is proposed. Extensive experimental results validate the analysis and proposed turn fault detection technique, demonstrating its effectiveness and robustness.

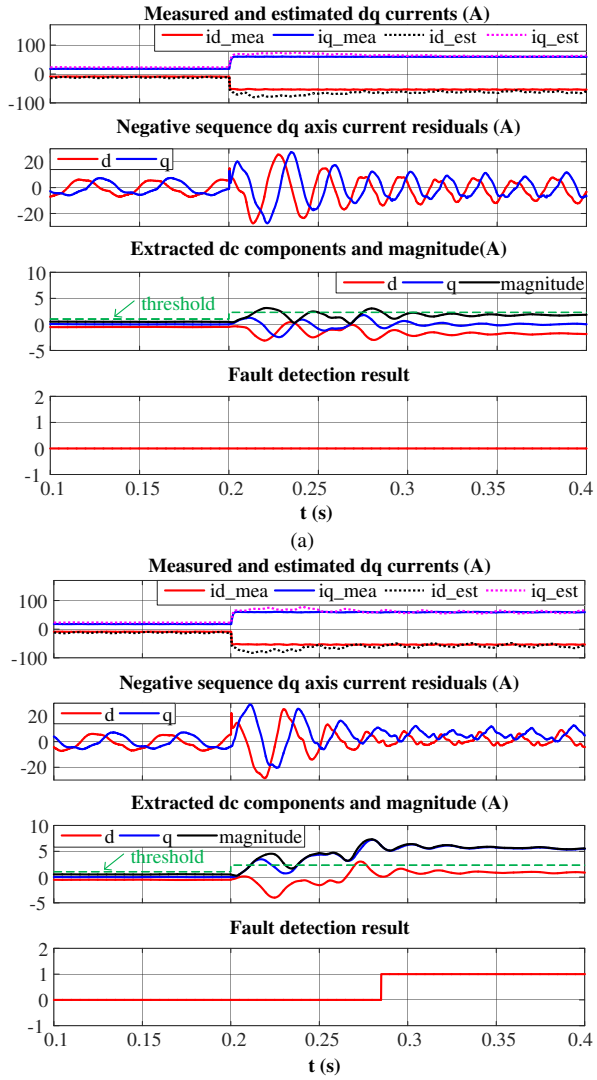

Fig. 15 The effect of current step change on the fault detection result in (a) healthy and (b) fault condition

References

[1] W. Cao, B. C. Mecrow, G. J. Atkinson, J. W. Bennett, and D. J. Atkinson, "Overview of electric motor technologies used for more electric aircraft (MEA)," *IEEE Trans. Ind. Electron.*, vol. 59, no. 9, pp. 3523–3531, 2012.

[2] Z. Q. Zhu and D. Howe, "Electrical Machines and Drives for Electric, Hybrid, and Fuel Cell Vehicles," *Proc. IEEE*, vol. 95, no. 4, pp. 746–765, 2007.

[3] IEEE, "Motor Reliability Working Group, Report of Large Motor Reliability Survey of Industrial and Commercial Installations," *IEEE Trans. Ind. Appl.*, vol. IA-4, July, no. 4, pp. 853–872, 1985.

[4] S. Grubic, J. M. Aller, B. Lu, and T. G. Habetler, "A survey on testing and monitoring methods for stator insulation systems of low-voltage induction machines focusing on turn insulation problems," *IEEE Trans. Ind. Electron.*, vol. 55, no. 12, pp. 4127–4136, 2008.

[5] A. Gandhi, T. Corrigan, and L. Parsa, "Recent advances in modeling and online detection of stator interturn faults in electrical motors," *IEEE Trans. Ind. Electron.*, vol. 58, no. 5, pp. 1564–1575, 2011.

[6] J. Faiz, H. Nejadi-koti, and Z. Valipour, "Comprehensive review on inter-turn fault indexes in permanent magnet motors," *IET Electr. Power Appl.*, vol. 11, no. 1, pp. 142–156, 2017.

[7] B. M. Ebrahimi, J. Faiz, and S. Member, "Feature Extraction for Short-Circuit Fault Detection in Permanent-Magnet Synchronous

Motors Using Stator-Current Monitoring," *IEEE Trans. Power Electron.*, vol. 25, no. 10, pp. 2673–2682, 2010.

[8] G. M. Joksimovic and J. Penman, "The detection of inter-turn short circuits in the stator windings of operating motors," *IEEE Trans. Ind. Electron.*, vol. 47, no. 5, pp. 1078–1084, 2000.

[9] H. Saavedra, J. C. Urresty, J. R. Riba, and L. Romeral, "Detection of interturn faults in PMSMs with different winding configurations," *Energy Convers. Manag.*, vol. 79, pp. 534–542, 2014.

[10] W. G. Zanardelli, E. G. Strangas, and S. Aviyente, "Identification of Intermittent Electrical and Mechanical Faults in Permanent Magnet AC Drives Based on Time-Frequency Analysis," *IEEE Trans. Ind. Appl.*, vol. 43, no. 4, pp. 1–10, 2007.

[11] J. A. Rosero, L. Romeral, J. A. Ortega, and E. Rosero, "Short-circuit detection by means of empirical mode decomposition and Wigner-Ville distribution for PMSM running under dynamic condition," *IEEE Trans. Ind. Electron.*, vol. 56, no. 11, pp. 4534–4547, 2009.

[12] C. Wang, X. Liu, and Z. Chen, "Incipient stator insulation fault detection of permanent magnet synchronous wind generators based on hilbert-huang transformation," *IEEE Trans. Magn.*, vol. 50, no. 11, 2014.

[13] K. H. Kim, "Simple online fault detecting scheme for short-circuited turn in a PMSM through current harmonic monitoring," *IEEE Trans. Ind. Electron.*, vol. 58, no. 6, pp. 2565–2568, 2011.

[14] Y. Mollet, X. Kestelyn, F. Meinguet, E. Semail, and J. Gyselinck, "Change-detection algorithm for short-circuit fault detection in closed-loop AC drives," *IET Electr. Power Appl.*, vol. 8, no. 5, pp. 165–177, 2014.

[15] B. Wang, J. Wang, A. Griffo, and B. Sen, "Stator Turn Fault Detection by Second Harmonic in Instantaneous Power for a Triple-Redundant Fault-Tolerant PM Drive," *IEEE Trans. Ind. Electron.*, vol. 65, no. 9, pp. 7279–7289, 2018.

[16] S. M. A. Cruz and A. J. Marques Cardoso, "Stator winding fault diagnosis in three-phase synchronous and asynchronous motors, by the extended park's vector approach," *IEEE Trans. Ind. Appl.*, vol. 37, no. 5, pp. 1227–1233, 2001.

[17] H. Jeong, S. Moon, and S. W. Kim, "An Early Stage Interturn Fault Diagnosis of PMSMs by Using Negative-Sequence Components," *IEEE Trans. Ind. Electron.*, vol. 64, no. 7, pp. 5701–5708, 2017.

[18] M. Zafarani, E. Bostanci, and Y. Qi, "Inter-turn Short Circuit Faults in Permanent Magnet Synchronous Machines : An Extended Review and Comprehensive Analysis," *IEEE J. Emerg. Sel. Top. Power Electron.*, vol. 6, no. 4, pp. 2173–2191, 2018.

[19] Y. Da, X. Shi, and M. Krishnamurthy, "A new approach to fault diagnostics for permanent magnet synchronous machines using electromagnetic signature analysis," *IEEE Trans. Power Electron.*, vol. 28, no. 8, pp. 4104–4112, 2013.

[20] F. Briz, M. W. Degner, A. Zamarron, and J. M. Guerrero, "On-line stator winding fault diagnosis in inverter-fed ac machines using high frequency signal injection," *IEEE Trans. Ind. Appl.*, vol. 39, no. 4, pp. 1109–1117, 2003.

[21] J. Hang, J. Zhang, M. Cheng, and J. Huang, "Online Inter-turn Fault Diagnosis of Permanent Magnet Synchronous Machine Using Zero Sequence Components," *IEEE Trans. Power Electron.*, vol. 30, no. 12, pp. 6731–6741, 2015.

[22] N. Leboeuf, T. Boileau, B. Nahid-Mobarakeh, G. Clerc, and F. Meibody-Tabar, "Real-time detection of interturn faults in PM drives using back-EMF estimation and residual analysis," *IEEE Trans. Ind. Appl.*, vol. 47, no. 6, pp. 2402–2412, 2011.

[23] S. Moon, H. Jeong, H. Lee, and S. W. Kim, "Interturn Short Fault Diagnosis in a PMSM by Voltage and Current Residual Analysis With the Faulty Winding Model," *IEEE Trans. Energy Convers.*, vol. 33, no. 1, pp. 190–198, 2018.

[24] R. M. Tallam, T. G. Habetler, and R. G. Harley, "Stator winding turn-fault detection for closed-loop induction motor drives," *IEEE Trans. Ind. Appl.*, vol. 39, no. 3, pp. 720–724, 2003.

[25] C. H. De Angelo, G. R. Bossio, and S. J. Giaccone, "Online model-based stator-fault detection and identification in induction motors," *IEEE Trans. Ind. Electron.*, vol. 56, no. 11, pp. 4671–4680, 2009.

[26] M. A. Mazzoletti, G. R. Bossio, C. H. De, and D. R. Espinoza-trejo, "A Model-Based Strategy for Interturn Short-Circuit Fault Diagnosis in PMSM," *IEEE Trans. Ind. Electron.*, vol. 64, no. 9, pp. 7218–7228, 2017.

[27] B. Vaseghi, B. Nahid-Mobarakh, N. Takorabet, and F. Meibody-Tabar, "Inductance identification and study of PM motor with winding turn short circuit fault," *IEEE Trans. Magn.*, vol. 47, no. 5, pp. 978–981, 2011.

[28] Y. Qi, E. Bostanci, V. Gurusamy, and B. Akin, "A Comprehensive Analysis of Short Circuit Current Behavior in PMSM Inter Turn Short Circuit Faults," *IEEE Trans. Power Electron.*, vol. 33, no. 12, pp. 10784–10793, 2018.

[29] X. Chen, J. Wang, B. Sen, P. Lazari, and T. Sun, "A high-fidelity and computationally efficient model for interior permanent-magnet machines considering the magnetic saturation, spatial harmonics, and iron loss effect," *IEEE Trans. Ind. Electron.*, vol. 62, no. 7, pp. 4044–4055, 2015.

[30] H. W. Kim, M. J. Youn, K. Y. Cho, and H. S. Kim, "Nonlinearity estimation and compensation of PWM VSI for PMSM under resistance and flux linkage uncertainty," *IEEE Trans. Control Syst. Technol.*, vol. 14, no. 4, pp. 589–601, 2006.